Eur. Phys. J. E **2**, 217–228 (2000)

THE EUROPEAN PHYSICAL JOURNAL E

EDP Sciences

Electron density modeling and reconstruction of infinite periodic minimal surfaces (IPMS) based phases in lipid-water systems. I. Modeling IPMS-based phases

P.E. Harper[a] and S.M. Gruner[b]

Department of Physics, Joseph Henry Laboratories, Jadwin Hall, Princeton University, Princeton NJ 08544 USA

Received 15 January 1999 and Received in final form 20 October 1999

Abstract. This is the first of two papers dealing with the structural solution of physical systems based on infinite periodic minimal surfaces (IPMS), such as surfactant, lipid-water, and block copolymer systems. In the first paper, the mathematics of minimal surfaces is briefly reviewed and details of the construction of the associate D, P, and G IPMS are described. Electron density models of lipid-water systems based on these IPMS are then constructed. The resulting models are then Fourier transformed to calculate the amplitudes of the first few Fourier terms. These amplitudes are then used to reconstruct the electron density which is examined and discussed. The subsequent paper will utilize the modeling results to aid in solving the structure of several real physical systems based on the D surface.

PACS. 61.30.Cz Theory and models of liquid crystal structure – 87.15.By Structure and bonding – 83.70.Jr Liquid crystals: nematic, cholesteric, smectic, discotic, etc.

1 Introduction

The first periodic surfaces with zero mean curvature were discovered in the 19th century. Among these were the D and P surfaces [1], members of a family of associate surfaces that was completed by the discovery of the G surface [2]. These elegant structures are both minimal, that is, having zero mean curvature everywhere, and periodic in all three dimensions, hence their name, infinite periodic minimal surfaces (IPMS). They remained a mathematical abstraction, albeit a beautiful one, until a century later when it was proposed that liquid crystal phases might be based on these surfaces [3]. It was postulated that amphiphile monolayers would be draped over both sides of the minimal surface with the remaining volume filled with water. A single liquid crystal would then be composed of a *single* bilayer that separates two distinct continuous systems of water channels, *i.e.*, bicontinuously. In recent years, X-ray diffraction consistent with the space group of these surfaces has been seen in a large variety of physical systems, from lipid-water mixtures [4,5] to block copolymers [6], to geological compounds such as zeolites [7].

The intriguing nature of these structures has also spawned a great deal of theoretical and experimental effort in recent years [8–15] and in the past [16–25]. Furthermore, there have been a number studies suggesting both the biological relevance and utility of these phases. It has been shown that small amounts of the channel protein alamethicin can induce the cubic phase [26] and it has been suggested that cubic structures may play a role in membrane fusion [27]. Cubic phases have also been used in the crystallization of membrane proteins [28] and as templates for the synthesis of mesoporous silica [29].

Despite the widespread interest and applicability of cubic phases, there have been few attempts at modeling or reconstructing these structures from X-ray diffraction information, due in no small measure to their mathematical complexity. For example, there have been a limited number of modeling [5] and reconstruction efforts [4,5,30] for D surface based systems.

In this paper, bilayer models of minimal surface based structures are created, Fourier transformed, and reconstructed. A detailed description of a straightforward method of constructing and Fourier transforming the models is described. The resulting Fourier amplitudes are then used to reconstruct the systems, which are examined *via* one-dimensional electron density cuts. These cuts offer a useful method of examining the reconstructions as interpretable by researchers with knowledge of one-dimensional bilayer structure. The work sets the stage for reconstruction of real lipid-water systems and for more detailed analysis of their structure, as described in a subsequent paper

[a] *Current address*: Department of Physics and Astronomy, Calvin College, 3201 Burton SE, Grand Rapids, MI 49546, USA.
e-mail: pharper@grand-canyon.edu

[b] *Current address*: Physics Department, Cornell University, 162 Clark Hall, Ithaca, NY 14853-2501, USA.
e-mail: smg26@cornell.edu

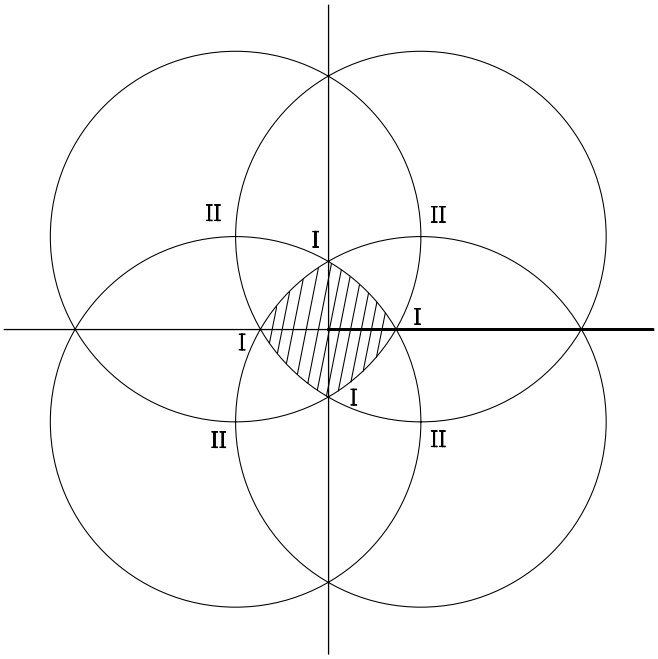

Fig. 1. Kreisbogenviereck (arc-quadrangle) in the complex plane for the D, P, and G surfaces. Each of the circles has a radius of $2^{1/2}$ and they are centered at $\pm 1/2^{1/2} \pm i1/2^{1/2}$, which are labeled II. The points of intersection labeled I are at $\pm(3^{1/2}-1)/2^{1/2}$ and $\pm i(3^{1/2}-1)/2^{1/2}$.

[31]. (Note: much of the work presented here may also be found the Ph.D. thesis of Paul Harper [32].)

2 Construction of minimal surfaces

This section contains a brief description of the construction of Schwarz's D and P surfaces and Schoen's G surface (see Tab. 1 for a listing of synonyms for these surfaces). The equations defining the minimal surfaces are given and a useful and highly accurate approximation to those equations is found. This approximate form allows the calculation of the coordinates for the minimal surfaces one to two orders of magnitude faster than if the original equations were used and it greatly reduces the amount of programming effort required to construct these surfaces. The section ends with a brief discussion of how the unit cells are formed by knitting together the fundamental pieces of the surfaces. A detailed description of the construction process can be found in [32]. Information on construction can also be found in [33].

Each of the D, P, and G surfaces is constructed by quilting together copies of a single elementary piece, or "Flächenstück" [35], for each surface. As the surfaces are associate, they share the same $R(w)$ and differ only in the association parameter θ (Tab. 2). To construct a Flächenstück for a given surface, one uses the appropriate association parameter and maps the area in complex space defined by the arc-quadrangle or "Kreisbogenviereck" [35], (see Fig. 1) into real space *via* the Weierstrass representation,

Table 1. Minimal surface names and space groups. Note that in the space group names that the bar across the three is often dropped in casual usage.

Name/Nickname	Single letter	Space group	
		Name	Number[a]
Double Diamond[b]	D or F[c]	$Pn\bar{3}m$	224
Plumber's Nightmare	P	$Im\bar{3}m$	229
Gyroid	G	$Ia\bar{3}d$	230

[a] International Tables of Crystallography [40].

[b] The double diamond surface is often referred in the polymer literature as OBDD, or ordered bicontinuous double diamond.

[c] The F designation originated with the discoverer of this surface [1]. The discoverer of the gyroid [2] renamed this surface (Schwarz's F surface) as the D surface. The latter designation seems more common in modern literature, though both labels are still in use. See [35] for an example in which *both* labels are used in the same paper!

Table 2. Parameters for the D, P and G surfaces. χ is the Euler characteristic for a unit cell, θ is the association parameter in radians, and A_0 is the surface area per a unit cell with sides of length 1 [48].

Surface	χ	θ	A_0
D	-2	0	1.919
P	-4	$\pi/2$	2.345
G	-8	0.66349	3.091

$$x(w) = \mathrm{Re}\int_0^w e^{i\theta}\left(1-w'^2\right)R(w')\,\mathrm{d}w', \tag{1}$$

$$y(w) = -\,\mathrm{Im}\int_0^w e^{i\theta}\left(1+w'^2\right)R(w')\,\mathrm{d}w', \tag{2}$$

$$z(w) = \mathrm{Re}\int_0^w e^{i\theta}\left(2w'\right)R(w')\,\mathrm{d}w', \tag{3}$$

where

$$R(w) = \frac{1}{(1-14w^4+w^8)^{1/2}}. \tag{4}$$

Note that $R(w)$ diverges at each of the corners of the Kreisbogenviereck, thus extra care must be taken in numerical evaluation of these formulas.

As the complex nature of the Kreisbogenviereck makes for an awkward parameterization and the integrals demand a fair amount of computational effort, both in computation time and programming, it is useful to make a highly accurate polynomial fit.

The function $(X(v,w),\ Y(v,w),\ Z(v,w))$, with $-1 \le v, w \le 1$, will give the coordinates for a given Flächenstück to an accuracy of 0.1%. The formula is given below:

$$(X(v,w),Y(v,w),Z(v,w)) = \mathrm{Re}\left[e^{i\theta}(X_{\mathrm{com}},Y_{\mathrm{com}},Z_{\mathrm{com}})\right], \tag{5}$$

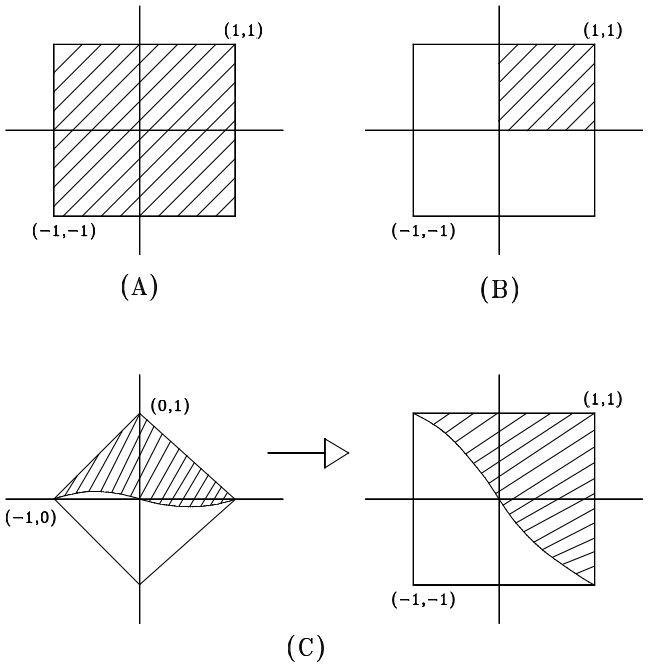

Fig. 2. (A) (v, w) coordinates for basic subsection of D surface, (B) (v, w) coordinates for basic subsection of P surface, (C) (g, h) coordinates for basic subsection of G surface (plot on left) and (v, w) coordinates for basic subsection of G surface (plot on right, rotated and enlarged version of plot on left) (see text).

where

$$\begin{aligned} X_{\text{com}} &= s + f(s,t)i, \\ Y_{\text{com}} &= t - f(-t,s)i, \\ Z_{\text{com}} &= 0.5(X_{\text{com}}^2 - Y_{\text{com}}^2) + 0.20659(X_{\text{com}}^4 - Y_{\text{com}}^4) \\ &\quad - 0.01268(X_{\text{com}}^6 - Y_{\text{com}}^6), \end{aligned} \tag{6}$$

where

$$\begin{aligned} f(s,t) = &-1.00102t + 2.00914s^2t - 0.69992s^4t \\ &- 5.19821s^6t - 0.62234t^3 - 1.18001s^2t^3 \\ &+ 28.34854s^4t^3 - 1.21488t^5 - 16.83032s^2t^5 \\ &+ 2.14239t^7 \end{aligned} \tag{7}$$

and

$$s = 0.298(v + w), \qquad t = 0.298(-v + w). \tag{8}$$

As a test of the accuracy of this formula, one can numerically compute the Euler characteristic by integrating the Gaussian curvature over the unit cell and comparing it to the known value. This was done by averaging the Gaussian curvatures for a 32×32 grid on the appropriate Flächenstück and multiplying by the number of Flächenstücke per unit cell. There are 6, 24, and 12 Flächenstücke per unit cell for the D, G, and P surfaces, respectively. As seen in Table 3, the values match up quite well. The integral of the Gaussian curvature over a Flächenstück is the same for each of the different surfaces; the different Euler constants for the unit cells of the different surfaces is a consequence of the varying number of Flächenstücke used in the construction of a given unit cell. In this paper, all calculations and graphs involving the D, G, and P surfaces are made using this approximation.

Table 3. Actual and approximated Euler characteristics (see text).

Surface	χ	χ_{calc}
D	-2	-1.996
P	-4	-4.008
G	-8	-8.005

The construction of the D cell begins with the basic Flächenstück ($-1 \le v,\ w \le 1$, see Fig. 2), which is scaled by a factor of 0.593207. By using symmetry operations from the appropriate space group, the rest of the cell is constructed. The construction of the P cell begins with the top quadrant of the Flächenstück ($0 \le v,\ w \le 1$, see Fig. 2) which is scaled by a factor of 0.463677. The cell is then constructed from symmetry operations on this basic piece, as shown in Figure 3.

The basic subsection for the G cell is more complex than the others. First, start with all $g,\ h$ such that

$$\begin{aligned} -1 \le g \le 1, \qquad & h \le 1 - |g|, \\ h \ge &-0.121906g + 0.052357g^3 + 0.101371g^5 \\ &+ 0.00310656g^7 - 0.0349283g^9. \end{aligned} \tag{9}$$

Then let $v = g + h$ and $w = -g + h$ for the plot (see Fig. 2). This basic piece is then scaled by 0.376472 and, as before, symmetry operations are used to build up the cell.

Finally, one should consider the family of surfaces that are associate to the D, P, and G surfaces. It turns out that most of these surfaces are not periodic; those that are periodic intersect themselves [2]. Additionally, one should be aware that there exist surfaces that are very similar to IPMS known as periodic nodal surfaces (PNS) and periodic zero potential surfaces (POPS) which are rather simple to calculate and quite interesting themselves [38].

3 Fourier transforms and bilayer modeling

In order to accurately reconstruct the electron density profile for a system, it is essential to calculate the amplitudes for a model of that system. This gives one a first guess at the proper phasing and a picture of what the profile should resemble. In this section, the Fourier amplitudes for a lipid bilayer centered on the D, P, and G minimal surfaces have been calculated. The bilayer models are then reconstructed using the Fourier amplitudes and examined using two representative cuts through the unit cells of each of the surfaces. Both cuts are normal to the minimal surface and one is through the points where the magnitude

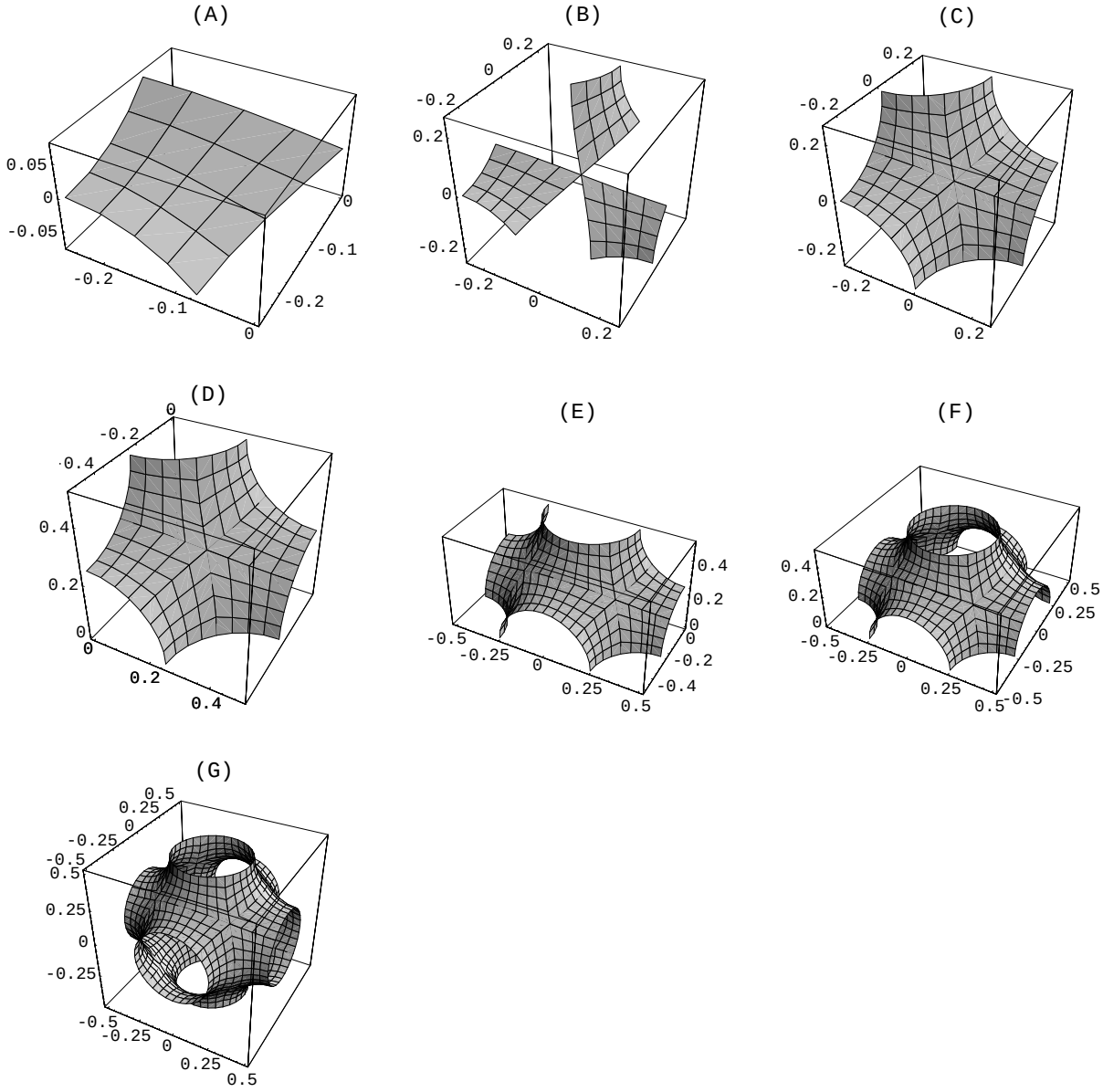

Fig. 3. (A) Basic subsection of the P surface, (B) three-fold symmetry applied to previous plot, (C) inversion symmetry applied to previous plot, (D) previous plot moved by (1/4, −1/4, 1/4), (E) inversion symmetry on x-axis applied to previous plot, (F) inversion symmetry on y-axis applied to previous plot, (G) inversion symmetry on z-axis applied to previous plot.

of the Gaussian curvature is the greatest and the other is through the points where the magnitude of Gaussian curvature is the least. Note that for these surfaces the minimum magnitude of Gaussian curvature is zero and hence the points of minimum magnitude of Gaussian curvature are locally flat. These cuts are quite useful, as they allow one to examine the bilayer at extremes of curvature. They also present a digestible portion of the electron density reconstruction, as a cut taken perpendicularly through a bilayer should resemble a simple lamellar reconstruction.

3.1 Fourier transform relationships

Several mathematical relations will be useful in calculating the Fourier transforms. The first takes advantage of the centrosymmetric nature of these structures. Let $V_{\rm tot}$ be the total structure, and V, $\bar{V}$ be the two halves of the structure related by inversion symmetry. One can write down Fourier transform of the structure and rewrite it in terms of one of the halves as follows:

$$F(V_{\rm tot}) \equiv \int_{V_{\rm tot}} e^{i\mathbf{q}\cdot\mathbf{x}}\,\mathrm{d}^3x = \int_V e^{i\mathbf{q}\cdot\mathbf{x}}\,\mathrm{d}^3x + \int_{\bar{V}} e^{i\mathbf{q}\cdot\mathbf{x}}\,\mathrm{d}^3x = \int_V e^{i\mathbf{q}\cdot\mathbf{x}}\,\mathrm{d}^3x + \int_V e^{-i\mathbf{q}\cdot\mathbf{x}}\,\mathrm{d}^3x = 2\,\mathrm{Re}\left[\int_V e^{i\mathbf{q}\cdot\mathbf{x}}\,\mathrm{d}^3x\right]. \quad (10)$$

Another useful relation known as the Abbé transformation [39] can be found using Gauss's divergence theorem, which states

$$\int_V \nabla^2\psi \, \mathrm{d}V = \oint_S \nabla\psi \cdot \mathrm{d}\mathbf{S}. \tag{11}$$

If one lets

$$\psi = e^{i\mathbf{q}\cdot\mathbf{x}}, \tag{12}$$

you have

$$-q^2 \int_V e^{i\mathbf{q}\cdot\mathbf{x}} \, \mathrm{d}V = \oint_S e^{i\mathbf{q}\cdot\mathbf{x}} i\mathbf{q} \cdot \mathrm{d}\mathbf{S}, \tag{13}$$

which can be solved to yield

$$F(V) = \int_V e^{i\mathbf{q}\cdot\mathbf{x}} \, \mathrm{d}V = \frac{-i}{q^2} \oint_S e^{i\mathbf{q}\cdot\mathbf{x}} \mathbf{q} \cdot \mathrm{d}\mathbf{S}, \tag{14}$$

thus reducing a volume integral to a surface integral. One can also calculate the volume enclosed by the surface by similar means. For this, one should choose $\psi = x^2+y^2+z^2$, giving

$$\int_V \mathrm{d}V = \frac{1}{3} \oint_S (x, y, z) \cdot \mathrm{d}\mathbf{S}, \tag{15}$$

yielding the volume enclosed by the surface in terms of a surface integral. If one knows the volume by another method, as is the case for the models used in this section, this offers a useful check on one's calculations.

3.2 Modeling lipid bilayers on IPMS

The simplest picture of this system is seen by simply draping a lipid monolayer over both sides of the appropriate minimal surface, or, equivalently, a lipid bilayer bisected by the minimal surface. Using the simple strip model of a bilayer shown in Figure 4, the amplitudes are calculated by the following formula:

$$\begin{aligned} F_{\text{bilayer}} = {} & \rho_{\text{water}} F_{\text{water}} + \rho_{\text{headgroup}} F_{\text{headgroup}} \\ & + \rho_{\text{tails}} F_{\text{tails}} + \rho_{\text{methyls}} F_{\text{methyls}}, \end{aligned} \tag{16}$$

where ρ_{water} is the electron density for water and F_{water} is the set of Fourier amplitudes of the volume occupied by water, etc. Since the F_{000} amplitude is not calculated, an arbitrary amount can be added to the electron densities. To make the calculation easier, the electron density of water is subtracted from all the electron densities, yielding

$$\begin{aligned} F_{\text{bilayer}} = {} & (\rho_{\text{headgroup}} - \rho_{\text{water}}) F_{\text{headgroup}} \\ & + (\rho_{\text{tails}} - \rho_{\text{water}}) F_{\text{tails}} \\ & + (\rho_{\text{methyls}} - \rho_{\text{water}}) F_{\text{methyls}}. \end{aligned} \tag{17}$$

Finally, this formula can be rewritten in terms of volumes bounded by interfaces on both sides of the minimal surface, *i.e.*, surfaces as

$$\begin{aligned} F_{\text{bilayer}} = {} & (\rho_{\text{headgroup}} - \rho_{\text{water}}) \\ & \times (F_{\text{water-headgroup}} - F_{\text{headgroup-tails}}) \\ & + (\rho_{\text{tails}} - \rho_{\text{water}})(F_{\text{headgroup-tails}} - F_{\text{tails-methyls}}) \\ & + (\rho_{\text{methyls}} - \rho_{\text{water}}) F_{\text{methyls}}, \end{aligned} \tag{18}$$

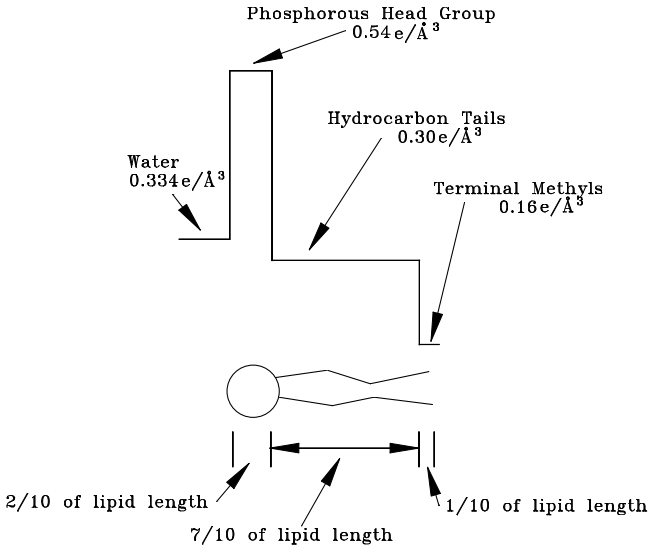

Fig. 4. Electron density model of a typical phospholipid used for calculating Fourier amplitudes for minimal surface based structures.

where $F_{\text{water-headgroup}}$ is the Fourier transform of the volume bounded by the water-headgroup interface, and so on. Now all that remains is to calculate the positions of these interfaces relative to the minimal surface.

It is assumed in these models that the distance is constant, and so the interface surface is modeled as a constant thickness surface, or a surface a constant distance away from the minimal surface. Note that a constant thickness surface is equivalent to a surface that is parallel to the minimal surface and can therefore equivalently be called a parallel interface surface. It is expected that the actual interface will be a compromise between constant thickness surface and a constant curvature surface. Since the variation in thickness for a constant curvature surface has been shown to be small (for a D surface based system), one expects that a constant thickness surface would give a reasonable approximation of the actual interface [16]. It is also important to note that the curvature of the bilayer should result in some sort of change in electron density. The next step in modeling these systems is to attempt to account for this variation; however, a simple strip model is a key first step and yields a decent match with experimental data for some systems [31]. For at least one D surface based system, it has been shown that the bilayer half thickness (monolayer thickness) is approximately 0.2 times the unit cell size [20]. Using this fact and the model in Figure 4, the monolayer thicknesses for the water-headgroup, headgroup-tails, and tails-methyls interfaces are calculated to be 0.2, 0.16, and 0.02 times the unit cell size, respectively. For the G and P surfaces, the monolayer thicknesses are calculated for a unit cell with the same average Gaussian curvature as the aforementioned D surface model. As an example, consider the D and G surfaces. Since the average Gaussian curvatures are equal, one has

$$\langle\kappa\rangle_{\text{D}} = \langle\kappa\rangle_{\text{G}} \tag{19}$$

Table 4. Fourier amplitudes for the constant thickness D surface models. $q(0,0,0)$ is the volume fraction for the unit cell. The monolayer thicknesses are given as a fraction of the unit cell.

Constant thickness D surface amplitudes				
q	Monolayer thickness			Bilayer model
	0.02	0.16	0.20	
$(0,0,0)$	0.0766	0.5791	0.6998	
$(1,1,0)$	0.0190	0.0996	0.0952	−1.00
$(1,1,1)$	0.0192	0.0870	0.0750	−1.12
$(2,0,0)$	−0.0103	−0.0311	−0.0168	0.71
$(2,1,1)$	0.0084	0.0173	0.0035	−0.59
$(2,2,0)$	0.0100	0.0087	−0.0093	−0.67
$(2,2,1)$	0.0109	0.0045	−0.0146	−0.69
$(3,1,0)$	−0.0073	−0.0002	0.0099	0.38
$(3,1,1)$	−0.0038	0.0010	0.0054	0.17
$(2,2,2)$	0.0112	−0.0081	−0.0233	−0.53
$(3,2,1)$	0.0037	−0.0043	−0.0075	−0.12
$(4,0,0)$	0.0055	−0.0071	−0.0078	−0.08
$(3,2,2)$	0.0071	−0.0115	−0.0123	−0.08

Table 5. Fourier amplitudes for the constant thickness P surface models. $q(0,0,0)$ is the volume fraction for the unit cell. The monolayer thicknesses are given as a fraction of the unit cell.

Constant thickness P surface amplitudes				
q	Monolayer thickness			Bilayer model
	0.016	0.13	0.16	
$(0,0,0)$	0.0749	0.5723	0.6812	
$(1,1,0)$	−0.0143	−0.0855	−0.0884	1.00
$(2,0,0)$	−0.0173	−0.0874	−0.0825	1.39
$(2,1,1)$	0.0144	0.0506	0.0348	−1.41
$(2,2,0)$	−0.0013	−0.0008	0.0011	0.11
$(3,1,0)$	0.0031	0.0056	0.0002	−0.33
$(2,2,2)$	−0.0127	−0.0120	0.0088	1.23
$(3,2,1)$	−0.0068	−0.0022	0.0090	0.62
$(4,0,0)$	0.0077	−0.0014	−0.0126	−0.62
$(3,3,0)$	0.0066	−0.0035	−0.0101	−0.40
$(4,1,1)$	−0.0075	0.0046	0.0136	0.50
$(4,2,0)$	0.0048	−0.0042	−0.0078	−0.23
$(3,3,2)$	0.0086	−0.0109	−0.0169	−0.37

and since

$$\langle \kappa \rangle = \frac{\int \kappa \, \mathrm{d}A}{\int \mathrm{d}A} = \frac{2\pi\chi}{a^2 A_0}, \tag{20}$$

one can say

$$\frac{2\pi\chi_\mathrm{D}}{a_\mathrm{D}^2 A_{0\mathrm{D}}} = \frac{2\pi\chi_\mathrm{G}}{a_\mathrm{G}^2 A_{0\mathrm{G}}}, \tag{21}$$

and therefore

$$\frac{a_\mathrm{G}}{a_\mathrm{D}} = \sqrt{\frac{\chi_\mathrm{G} A_{0\mathrm{D}}}{\chi_\mathrm{D} A_{0\mathrm{G}}}} \cong 1.58, \tag{22}$$

where χ is the Euler characteristic, A_0 is the surface area per unit cell for the appropriate surface (see Tab. 2 for values) and a_D, a_G are the cell dimensions for the D and G surfaces, respectively. After doing the above calculation for the D and P surfaces as well, it is found that surfaces with the same average Gaussian curvature have cell dimensions $d_\mathrm{D} : d_\mathrm{P} : d_\mathrm{G}$ in the ratio of $1 : 1.28 : 1.58$, which have been calculated by others [41]. Therefore, for a fixed lipid length and a unit cell, the ratios of the lipid length per cell dimension for these surfaces would be $\frac{l}{d_\mathrm{D}} : \frac{l}{d_\mathrm{P}} : \frac{l}{d_\mathrm{G}}$, or $1 : 0.78 : 0.63$. Hence, as the monolayer thicknesses for the constant thickness surfaces bounded by the water-headgroup, headgroup-tails, and tails-methyls interfaces for the D surface are 0.2, 0.16, and 0.02, the corresponding monolayer thicknesses are approximately 0.16, 0.13, 0.016 for the P surface and 0.13, 0.10, 0.013 for the G surface.

Table 6. Fourier amplitudes for the constant thickness G surface models. $q(0,0,0)$ is the volume fraction for the unit cell. The monolayer thicknesses are given as a fraction of the unit cell.

Constant thickness G surface amplitudes				
q	Monolayer thickness			Bilayer model
	0.013	0.10	0.13	
$(0,0,0)$	0.0802	0.5841	0.7294	
$(2,1,1)$	0.0170	0.0804	0.0704	−1.00
$(2,2,0)$	0.0116	0.0515	0.0430	−0.70
$(3,2,1)$	−0.0024	−0.0052	−0.0013	0.17
$(4,0,0)$	−0.0092	−0.0153	0.0018	0.67
$(4,2,0)$	−0.0086	−0.0077	0.0086	0.60
$(3,3,2)$	0.0118	0.0067	−0.0167	−0.83
$(4,2,2)$	0.0071	0.0013	−0.0127	−0.48
$(4,3,1)$	0.0053	0.0000	−0.0096	−0.33
$(5,2,1)$	−0.0019	0.0006	0.0025	−0.08
$(4,4,0)$	−0.0015	0.0007	0.0010	0.03
$(5,3,2)$	−0.0026	0.0029	0.0037	0.05
$(6,1,1)$	−0.0061	0.0074	0.0098	0.13

Once the surface is defined, it is first broken up into triangles, which are in turn broken up into right triangles. The Abbé transformation is used to turn the Fourier transform of the volume bounded by this surface into a surface integral. This surface integral is then evaluated over the right triangles that make up the surface. Apart from a multiplicative constant, the surface integral for each of the right triangles is essentially the Fourier transform of the triangle. The integral for a given triangle is simplified by rotating and translating the coordinates so that the legs of the right triangle lie along the x-and y-axes. The Fourier transform of this triangle is then given by

$$\int_0^b \int_0^{-(a/b)y+a} e^{iq_x x+iq_y y}\,\mathrm{d}x\,\mathrm{d}y = \frac{ae^{ibq_y}}{aq_xq_y - bq_y^2} - \frac{be^{iaq_x}}{aq_x^2 - bq_xq_y} - \frac{1}{q_xq_y}, \quad (23)$$

where a and b are, respectively, the lengths of the legs along the x- and y-axes, $q_x,\ q_y \neq 0$ and $aq_x - bq_y \neq 0$.

The results of the calculations are listed in Tables 4, 5, and 6, for the D, P, and G surfaces, respectively. The first column in these tables lists the amplitudes for which the Fourier transforms are calculated. The next three columns contain, respectively, the amplitudes for the volume bounded by the tail-methyl interface, the tail-headgroup interface, and the headgroup-water interface. Next, these amplitudes and equation (18) are used to calculate the model bilayer amplitudes. The final column of each of the tables contains the model bilayer amplitudes, with the first non-zero amplitude normalized to one.

For these calculations, the basic unit was divided up into a 16×16 grid for the constant thickness surfaces. For the Fourier transformations of the minimal surfaces themselves, each Flächenstück was divided up into a 32×32 grid. Moving to a finer grid did not significantly change the results. For example, if a 32×32 grid is used in calculating the Fourier amplitudes for the constant thickness D surface with a monolayer thickness of 0.2 (see Tab. 4), less than a 0.1% variation is seen in the $q = (0,0,0)$ amplitude and a variation of about 0.0001 or less is seen in the remaining amplitudes. The results are shown in Tables 7, 8, and 9 for the D, P, and G surfaces, respectively, Note the good agreement with values previously calculated [34, 36,37]. A discussion of these results is deferred until the section on reconstruction of these models.

Table 7. Fourier amplitudes for a unit cell of the D surface. $q(0,0,0)$ is the surface area of a unit cell.

D surface Fourier amplitudes			
q	This work[a]	Anderson [37]	Mackay [34]
$(0,0,0)$	1.91925	1.91928	1.9193
$(1,1,0)$	0.4784	0.4780	0.4775
$(1,1,1)$	0.4840	0.4840	0.4866
$(2,0,0)$	−0.2612	−0.2610	−0.2564
$(2,1,1)$	0.2124		0.2129
$(2,2,0)$	0.2567		0.2578
$(2,2,1)$	0.2793		0.2789
$(3,1,0)$	−0.1881		−0.1877
$(3,1,1)$	−0.0981		−0.0946
$(2,2,2)$	0.2904		0.2960
$(3,2,1)$	0.0963		0.0952
$(4,0,0)$	0.1435		0.1458
$(3,2,2)$	0.1865		

[a] 32×32 grid on each Flächenstück.

3.3 Reconstructions of models

Once one has the Fourier amplitudes, one can calculate the electron density using the following formulas, taken from [40]. For $Pn\bar{3}m$ symmetry, D surface symmetry, the

Table 8. Fourier amplitudes for a unit cell of the P surface. $q(0,0,0)$ is the surface area of a unit cell.

P surface Fourier amplitudes		
q	This work[a]	Anderson [37]
$(0,0,0)$	2.34587	2.345107
$(1,1,0)$	−0.44939	−0.44936
$(2,0,0)$	−0.54525	−0.54494
$(2,1,1)$	0.45616	0.45618
$(2,2,0)$	−0.04179	−0.04256
$(3,1,0)$	0.09868	0.09885
$(2,2,2)$	−0.40537	−0.40418
$(3,2,1)$	−0.21770	−0.21779
$(4,0,0)$	0.24715	
$(3,3,0)$	0.21536	
$(4,1,1)$	−0.24289	
$(4,2,0)$	0.15695	
$(3,3,2)$	0.27878	

[a] 32×32 grid on each Flächenstück.

Table 9. Fourier amplitudes for a unit cell of the G surface. $q(0,0,0)$ is the surface area of a unit cell.

G surface Fourier amplitudes		
q	This work[a]	Clerc [36]
$(0,0,0)$	3.0926	
$(2,1,1)$	0.6607	0.660
$(2,2,0)$	0.4498	0.451
$(3,2,1)$	−0.0922	−0.092
$(4,0,0)$	−0.3612	−0.360
$(4,2,0)$	−0.3382	−0.338
$(3,3,2)$	0.4671	0.467
$(4,2,2)$	0.2812	0.282
$(4,3,1)$	0.2094	0.209
$(5,2,1)$	−0.0776	−0.077
$(4,4,0)$	−0.0604	−0.060
$(5,3,2)$	−0.1038	−0.104
$(6,1,1)$	−0.2451	−0.245

[a] 32 × 32 grid on each Flächenstück.

electron density is given by

see equation (24) *on next page*

The formula for $\mathrm{Im}\,\bar{3}\mathrm{m}$ symmetry (P surface symmetry) is much simpler, and is given by

$$\rho(x,y,z) = \sum_{h=0}^{\infty}{}' \sum_{k=0}^{\infty}{}' \sum_{l=0}^{\infty}{}' F_{hkl} \cos(2\pi hx) \times \cos(2\pi ky) \cos(2\pi lz). \quad (25)$$

For $\mathrm{Ia}\bar{3}\mathrm{d}$ symmetry (G surface symmetry), the electron density is

see equation (26) *on next page*

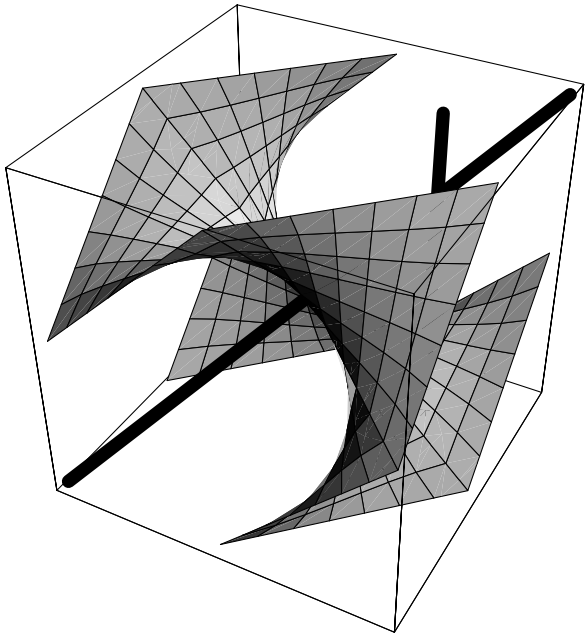

Fig. 5. D surface unit cell with lines drawn through the points of maximum and minimum magnitude of Gaussian curvature. The body diagonal (111) goes through the points where the magnitude of Gaussian curvature is minimal and the vertical line (001) goes through the points where the magnitude of Gaussian curvature is maximal. Both lines are normal to the surface at the intersection points.

Note that the primed summation indicates that the $n = 0$ term of the summation should be multiplied by $\frac{1}{2}$, a convention followed throughout this series of papers. For all three of these surfaces, the amplitudes satisfy the condition $F_{hkl} = F_{lhk} = F_{klh}$. For the D and P surfaces, they also satisfy $F_{hkl} = F_{hlk}$. For the G surface the situation is slightly more complex, as $F_{hkl} = F_{hlk}$ only for $h+k+l = 4n$ and $F_{hkl} = -F_{hlk}$ for $h+k+l = 4n+2$.

Once one has reconstructed the electron density, it can be examined in order to gain intuition about what one should expect to see from a reconstruction of actual data. Two-dimensional cross-sections are extraordinarily difficult to interpret and convey little information about important parameters such as the thickness of the bilayer and information about the varying structure of the bilayer at points of differing curvature; one-dimensional cuts through the surface offer much more useful information. In all three of these surfaces, a cut along the body diagonal (111) will normally intersect the surface at its flat points, or points of zero Gaussian curvature. As the Gaussian curvature at all points on these surfaces is less than or equal to zero, this represents one extreme in curvature. If one then makes an appropriately selected vertical cut (001), one normally intersects the points on the surface with a maximum magnitude of Gaussian curvature. The location of these cuts for each of the surfaces are shown in Figure 5, 6, and 7 for the D, P, and G surfaces.

For the bilayer model based on a D surface, the electron density profile cuts are shown in Figure 8. The top

$$\begin{aligned}\rho(x,y,z) = &\sum_{h=0}^{\infty}{}'\sum_{k=0}^{\infty}{}'\sum_{l=0}^{\infty}{}' F_{hkl}^{(h+k=2n,k+l=2n)} \cos(2\pi hx)\cos(2\pi ky)\cos(2\pi lz)\\ &- \sum_{h=0}^{\infty}{}'\sum_{k=0}^{\infty}{}'\sum_{l=0}^{\infty}{}' F_{hkl}^{(h+k=2n,k+l=2n+1)} \sin(2\pi hx)\sin(2\pi ky)\cos(2\pi lz)\\ &- \sum_{h=0}^{\infty}{}'\sum_{k=0}^{\infty}{}'\sum_{l=0}^{\infty}{}' F_{hkl}^{(h+k=2n+1,k+l=2n)} \cos(2\pi hx)\sin(2\pi ky)\sin(2\pi lz)\\ &- \sum_{h=0}^{\infty}{}'\sum_{k=0}^{\infty}{}'\sum_{l=0}^{\infty}{}' F_{hkl}^{(h+k=2n+1,k+l=2n+1)} \sin(2\pi hx)\cos(2\pi ky)\sin(2\pi lz). \end{aligned} \tag{24}$$

$$\begin{aligned}\rho(x,y,z) = &\sum_{h=0}^{\infty}{}'\sum_{k=0}^{\infty}{}'\sum_{l=0}^{\infty}{}' F_{hkl}^{(h+k=2n,k+l=2n)} \cos(2\pi hx)\cos(2\pi ky)\cos(2\pi lz)\\ &- \sum_{h=0}^{\infty}{}'\sum_{k=0}^{\infty}{}'\sum_{l=0}^{\infty}{}' F_{hkl}^{(h+k=2n,k+l=2n+1)} \sin(2\pi hx)\cos(2\pi ky)\sin(2\pi lz)\\ &- \sum_{h=0}^{\infty}{}'\sum_{k=0}^{\infty}{}'\sum_{l=0}^{\infty}{}' F_{hkl}^{(h+k=2n+1,k+l=2n)} \sin(2\pi hx)\sin(2\pi ky)\cos(2\pi lz)\\ &- \sum_{h=0}^{\infty}{}'\sum_{k=0}^{\infty}{}'\sum_{l=0}^{\infty}{}' F_{hkl}^{(h+k=2n+1,k+l=2n+1)} \cos(2\pi hx)\sin(2\pi ky)\sin(2\pi lz). \end{aligned} \tag{26}$$

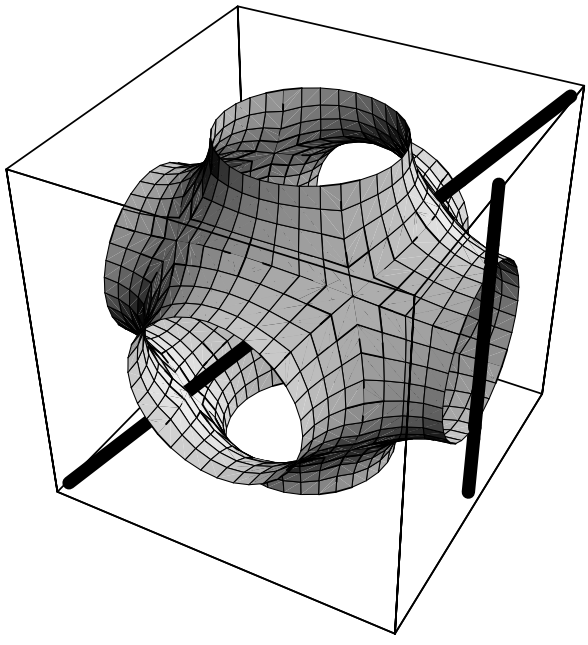

Fig. 6. P surface unit cell with lines drawn through the points of maximum and minimum magnitude of Gaussian curvature. The body diagonal (111) goes through the points where the magnitude of Gaussian curvature is minimal and the vertical line (001) goes through the points where the magnitude of Gaussian curvature is maximal. Both lines intersect the surface at right angles.

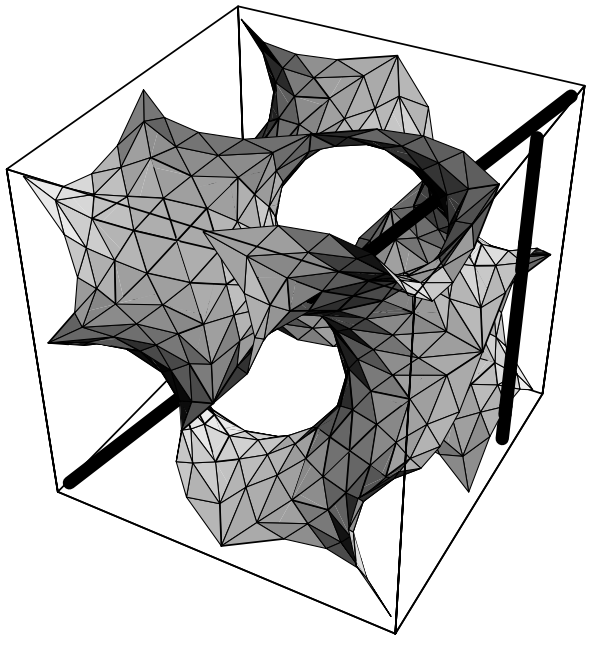

Fig. 7. G surface unit cell with lines drawn through the points of maximum and minimum magnitude of Gaussian curvature. The body diagonal (111) goes through the points where the magnitude of Gaussian curvature is minimal and the vertical line (001) goes through the points where the magnitude of Gaussian curvature is maximal. Both lines intersect the surface at right angles.

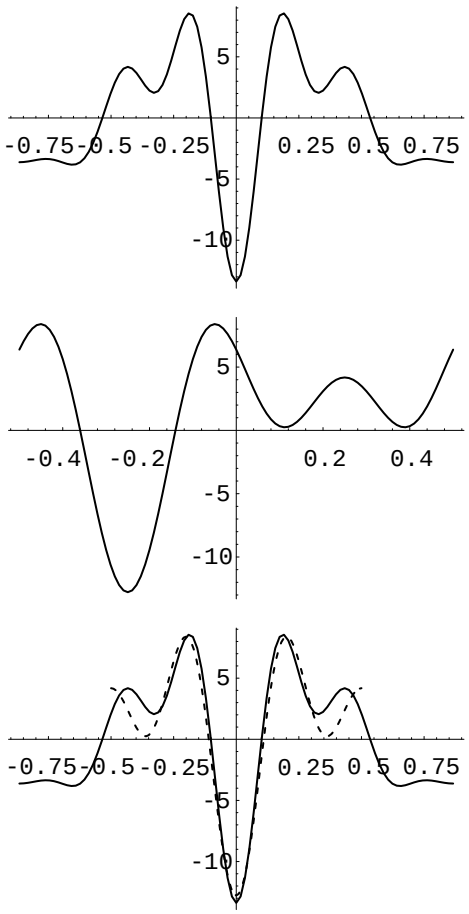

Fig. 8. Plots of model bilayer electron density for the D surface. The y-axis is electron density in arbitrary units and the x-axis is position along a cut line. Top view: cut along line through points of zero Gaussian curvature. Middle view: cut along line through points of maximum magnitude of Gaussian curvature. See the previous figure for a plot of these lines on a unit cell of the D surface. Bottom view: overlay of bilayer from above views on the same horizontal scale. Solid line is from top view and dashed line is from the middle view, where the middle view has been horizontally shifted so the minima coincide.

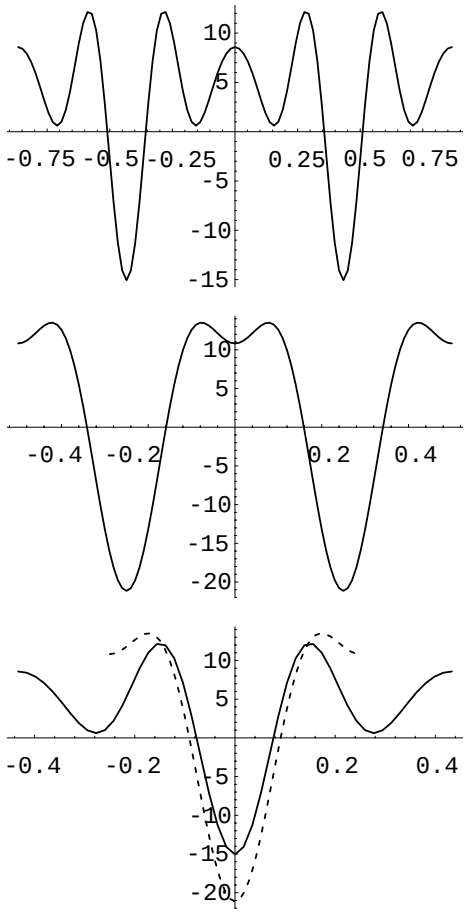

Fig. 9. Plots of model bilayer electron density for the P surface. The y-axis is electron density in arbitrary units and the x-axis is position along a cut line. Top view: cut along line through points of zero Gaussian curvature. Middle view: cut along line through points of maximum magnitude of Gaussian curvature. See the previous figure for a plot of these lines on a unit cell of the P surface. Bottom view: overlay of bilayer from above views on the same horizontal scale. Solid line is from top view and dashed line is from the middle view, where the middle view has been horizontally shifted so the minima coincide.

plot is an electron density profile through the body diagonal (111), which normally intersects the bilayer at its flat point. The deep methyl trough is in the middle of the plot and is immediately bounded by the peaks due to the phosphorus headgroups. For these systems, the deepest minima are methyl troughs and the greatest maxima are the phosphorus headgroups, similar to the diffraction seen in lamellar systems [42].

The region outside the bilayer is filled with water and ideally would yield a flat line. The bumps that are seen at the edges are due to the limited resolution of the reconstruction. Though for this phospholipid model the bumps are a minor feature, it will be shown in a subsequent paper [31] that these spurious bumps are major features of the reconstruction of non-phospholipids such as mono-olein. The bottom plot is a profile of the electron density through the bilayer at its points of extreme curvature (001). As the top plot, the methyl trough is clearly defined and is bounded by the dominant methyl peaks. Outside of the peaks is the water region which contains a bump reminiscent of the bump found in the water region of a reconstruction of the H_{II} phase of DOPE [43]. It is important to be aware of these artifacts in the water region in order to properly reconstruct and interpret systems based on a D surface.

For the bilayer model based on a P surface, the electron density profile cuts are shown in Figure 9. The top plot is an electron density profile through the body diagonal (111), which normally intersects the bilayer twice, both times at flat points in the bilayer. The deep methyl troughs bounded by the phosphorus headgroup peaks can be seen on the left and right sides of the plot. The water

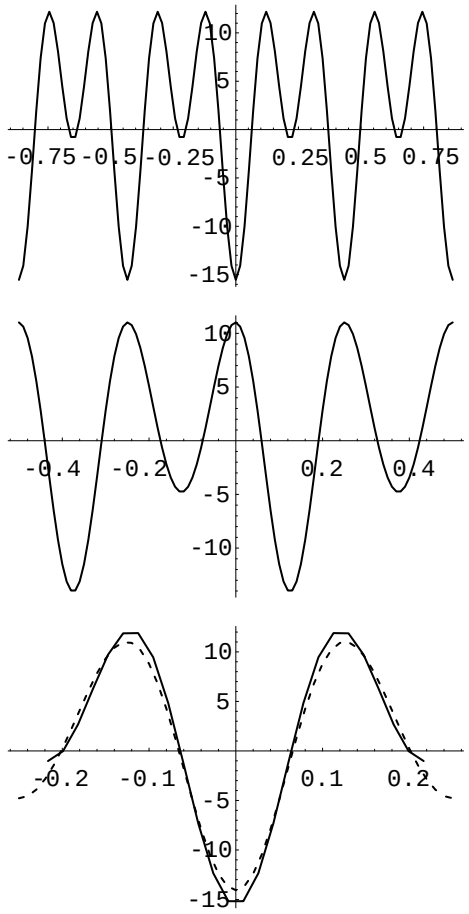

Fig. 10. Plots of model bilayer electron density for the G surface. The y-axis is electron density in arbitrary units and the x-axis is position along a cut line. Top view: cut along line through points of zero Gaussian curvature. Middle view: cut along line through points of maximum magnitude of Gaussian curvature. See the previous figure for a plot of these lines on a unit cell of the G surface. Bottom view: overlay of bilayer from above views on the same horizontal scale. Solid line is from top view and dashed line is from the middle view, where the middle view has been horizontally shifted so the minima coincide.

regions in between the bilayers each contain a bump due to the low resolution of the reconstructions. The bottom plot is an electron density cut through the bilayer at two points of extreme curvature (001). The methyl troughs are well defined and the headgroup peaks are close enough to partially overlap. The close proximity of the headgroups suggests that one is unlikely to find an experimental example corresponding to this model.

For the bilayer model based on the G surface, the electron density profile cuts are shown in Figure 10. The top plot is an electron density profile through the body diagonal (111), which normally intersects the bilayer five times, each time through a flat point on the bilayer. The methyl troughs are clear, as are the phosphorous peaks. The bottom plot shows a cut through the bilayer at two points of extreme curvature (001). As with the top plot, the methyl troughs and phosphorous peaks are quite clear and there are no artifacts in the water region. It is then rather ironic that though the G surface is the most difficult of these three minimal surfaces to construct, it is the most straightforward to reconstruct, as one does not encounter the artifacts present in the others.

4 Conclusions

The complexity of the minimal surfaces makes for a nontrivial computational challenge. The computationally accessible methods detailed in this paper facilitate the application of IPMS for the description and modeling of physical systems. Another factor that has hindered the application of IPMS to physical systems is the difficulty of interpreting the traditional planar cross-sectional views of the 3-dimensional surfaces. The linear profile method used here is based on the recognition that the bilayers are readily interpreted in terms of 1-dimensional density profiles. Another advantage of the linear profiles are that they allow ready comparison of the bilayer structure at the extremes of the curvature present in the system. In so far as variation in bilayer structure in a mesomorph is a factor in the stability of the phase [11,16], comparison of the magnitude of variation at the curvature extremes helps to understand the phase sequences and occurrences of different structures. A final aspect of the modeling described above is the explicit identification of artifacts resulting from the low resolution of the Fourier reconstructions. The limited resolution of the diffraction data from many complex mesomorphs forces the use of low resolution reconstructions. It is important to realize that it is possible to locate major features of a bilayer to distances far below the resolution of the reconstruction, as has been done in [43]. As there are no attempts to locate features to such precision in this paper, a justification of such reconstructions will not be given; the interested reader is referred to an excellent discussion of the practical limits of resolution in [44].

Future modeling and reconstruction efforts should seek to analyze the position of the lipid-water interface, as has been done for the inverse hexagonal phase [43]. It is generally accepted that lipid mesomorphic behavior is strongly dependent on a competition between monolayer bending and chain packing free energies [16,19,45]. Although phenomenological forms for the bending [46] and chain packing [47] forms have been proposed, there is little information about the range of validity of these forms as a function of monolayer curvature and resultant thickness variations. Minimal surface based phases offer the possibility to examine the competition between curvature and packing, since the curvature of constant thickness models varies substantially as one ranges across the structure. If the thickness of the bilayer as a function of curvature in real systems can be extracted from reconstructions, then it may be possible to gain insight as to the functional forms of the curvature and packing energies, which would aid in the understanding of mesomorphs based on minimal surface morphologies.

We are grateful for a National Science Foundation Fellowship and Liposome Co. Fellowship for P.H. and for support from the D.O.E. (grant DE-FG02-87-ER60522).

References

1. H.A. Schwarz, *Gesammelte Mathematische Abhandlungen* (Springer, Berlin, 1890).
2. A.H. Schoen, NASA Tech. Rep. No. 05541, 1970.
3. L.E. Scriven, Nature (London) **266**, 123 (1976).
4. P. Mariani, H. Delacroix, V. Luzzati, J. Mol. Biol. **204**, 165 (1988).
5. W. Longley, T.J. McIntosh, Nature **303**, 612 (1983).
6. D.A. Hajduk, P.E. Harper, S.M. Gruner, C.C. Honeker, G. Kim, E.L. Thomas, L.J. Fetters, Macromolecules **27**, 4063 (1994).
7. S. Andersson, S.T. Hyde, H.G. von Schnering, Z. Kristallogr. **168**, 1 (1984).
8. A. Fogden, S.T. Hyde, Eur. Phys. J. B **7**, 91 (1999).
9. C. Neto, G. Aloisi, P. Baglioni, K. Larsson, J. Phys. Chem. B **103**, 3896 (1999).
10. R.H. Templer, Curr. Opin. Colloid In. **3**, 255 (1998).
11. R.H. Templer, J.M. Seddon, N.A. Warrender, A. Syrykh, Z. Huang, R. Winter, J. Erbes, J. Phys. Chem. B **102**, 7251 (1998).
12. R.H. Templer, J.M. Seddon, P.M. Duesing, R. Winter, J. Erbes, J. Phys. Chem. B **102**, 7262 (1998).
13. R.H. Templer, B.J. Khoo, J.M. Seddon, Langmuir **14**, 7427 (1998).
14. J.H. Laurer, D.A. Hajduk, J.C. Fung, J.W. Sedat, S.D. Smith, S.M. Gruner, D.A. Agard, R.J. Spontak, Macromol. **30**, 3938 (1997).
15. P. Alexandridis, U. Olsson, B. Lindman, Langmuir **14**, 2627 (1998).
16. D.M. Anderson, S.M. Gruner, S. Leibler, Proc. Natl. Acad. Sci. **85**, 5364 (1988).
17. S.T. Hyde, J. Phys. Chem. **93**, 1458 (1989).
18. K. Larsson, J. Phys. Chem. **93**, 7304 (1989).
19. W. Helfrich, H. Rennschuh, J. Phys. (Paris) **23**, C7, 189 (1990).
20. D.C. Turner, Z.-G. Wang, S.M. Gruner, D.A. Mannock, R.N. McElhaney, J. Phys. II France **2**, 2039 (1992).
21. S. Ljunggren, J.C. Eriksson, Langmuir **8**, 1300 (1992).
22. V. Luzzati, J. Phys. II France **5**, 1649 (1995).
23. R. Templer, D.C. Turner, P. Harper, J.M. Seddon, J. Phys. II France **5**, 1053 (1995).
24. C. Czeslik, R. Winter, G. Rapp, K. Bartels, Biophys. J. **68**, 1423 (1995).
25. S. Andersson, M. Jacob, S. Lidin, K. Larsson, Z. Kristallogr. **210**, 315 (1995).
26. S.L. Keller, S.M. Gruner, K. Gawrisch, Biochim. Biophys. Acta **1278**, 241 (1996).
27. J.L. Nieva, A. Alonso, G. Basanez, F.M. Goni, A. Gulik, R. Vargas, V. Luzzati, FEBS Lett. **368**, 143 (1995).
28. E.M. Landau, J.P. Rosenbusch, Proc. Natl. Acad. Sci. USA **93**, 14532 (1996).
29. G.S. Attard, J.C. Glyde, C.G. Goltner, Nature **378**, 366 (1995).
30. V. Luzzati, P. Mariani, H. Delacroix, Makromol. Chem., Macromol Symp. **15**, 1 (1988).
31. P.E. Harper, S.M. Gruner, this issue, p. 229.
32. P.E. Harper, Ph.D. thesis, Princeton University, 1996.
33. H. Terrones, J. Phys. (Paris) **23**, C7, 7345 (1990).
34. A.L. Mackay, Nature **314**, 604 (1985).
35. S. Andersson, S.T. Hyde, K. Larsson, S. Lidin, Chem. Rev. **88**, 221 (1988).
36. M. Clerc, E. Dubois-Violette, J. Phys. II France **4**, 275 (1994).
37. D.M. Anderson, H.T. Davis, L.E. Scriven, J.C.C. Nitsche, *Advances in Chemical Physics - Periodic Surfaces of Mean Curvature* (John Wiley and Sons Inc., 1990).
38. H.G. von Schnering, R. Nesper, Z. Phys. B **85**, 407 (1991).
39. R. Hosemann, S.N. Bagchi, *Direct Analysis of Diffraction by Matter* (North-Holland Pub. Co., 1962).
40. N.F.M Henry, K. Lonsdale (editors), *International Tables for X-ray Crystallography,* Vol. **I** (Kynoch Press, Birmingham England, 1969).
41. S.T. Hyde, S. Andersson, Z. Kristallogr. **168**, 213 (1984).
42. M.C. Wiener, S.H. White, Biophys. J. **61**, 434 (1992).
43. D.C. Turner, S.M. Gruner, Biochem. **31**, 1340 (1992).
44. M.C. Wiener, S.H. White, Biophys. J. **59**, 162 (1991).
45. G.L Kirk, S.M. Gruner, J. Phys. France **46**, 761 (1985).
46. W. Helfrich, Z. Naturforsch. C **28**, 693 (1973).
47. P.M. Duesing, R.H. Templer, J.M. Seddon, Langmuir **13**, 351 (1997).
48. D. Anderson, H. Wennerstrom, U. Olsson, J. Phys. Chem. **93**, 4243 (1989).